

Feasibility study of the positronium imaging with the J-PET tomograph

P. Moskal¹, D. Kisielewska¹, C. Curceanu², E. Czerwiński¹, K. Dulski¹,
 A. Gajos¹, M. Gorgol³, B. Hiesmayr⁴, B. Jasińska³, K. Kacprzak¹,
 Ł. Kapłon¹, G. Korcyl¹, P. Kowalski⁵, W. Krzemień⁶, T. Kozik¹,
 E. Kubicz¹, M. Mohammed^{1,7}, Sz. Niedźwiecki¹, M. Pałka¹,
 M. Pawlik-Niedźwiecka¹, L. Raczyński⁵, J. Raj¹, S. Sharma¹, Shivani¹,
 R. Y. Shopa⁵, M. Silarski¹, M. Skurzok¹, E. Stępień¹, W. Wiślicki⁵,
 B. Zgardzińska³

¹ Faculty of Physics, Astronomy and Applied Computer Science,
 Jagiellonian University, 30-348 Cracow, Poland

² INFN, Laboratori Nazionali di Frascati, 00044 Frascati, Italy.

³ Institute of Physics, Maria Curie-Skłodowska University, 20-031 Lublin,
 Poland

⁴ Faculty of Physics, University of Vienna, 1090 Vienna, Austria

⁵ Department of Complex Systems, National Centre for Nuclear Research,
 05-400 Otwock-Świerk, Poland

⁶ High Energy Physics Division, National Centre for Nuclear Research,
 05-400 Otwock-Świerk, Poland

⁷ Department of Physics, College of Education for Pure Sciences,
 University of Mosul, Mosul, Iraq

Abstract. A detection system of the conventional PET tomograph is set-up to record data from e^+e^- annihilation into two photons with energy of 511 keV, and it gives information on the density distribution of a radiopharmaceutical in the body of the object. In this paper we explore the possibility of performing the three gamma photons imaging based on ortho-positronium annihilation, as well as the possibility of positronium mean lifetime imaging with the J-PET tomograph constructed from plastic scintillators. For this purposes simulations of the ortho-positronium formation and its annihilation into three photons were performed taking into account distributions of photons' momenta as predicted by the theory of quantum electrodynamics and the response of the J-PET tomograph. In order to test the proposed ortho-positronium lifetime image reconstruction method, we concentrate on the decay of the ortho-positronium into three photons and applications of radiopharmaceuticals labeled with isotopes emitting a prompt gamma. The proposed method of imaging is based on the determination of hit-times and hit-positions of registered photons which enables the reconstruction of the time and position of the annihilation point as well as the lifetime of the ortho-positronium on an event-by-event basis. We have simulated the production of the positronium in point-like sources and in a cylindrical phantom composed of a set of different materials in which the ortho-positronium lifetime varied from 2.0 ns to 3.0 ns, as expected for ortho-positronium created in the human body. The presented reconstruction method for total-body J-PET like detector allows to achieve a mean lifetime resolution of ~ 40 ps. Recent Positron Annihilation Lifetime Spectroscopy measurements of cancerous and healthy uterine tissues show that this sensitivity may allow to study the morphological changes in cell structures.

1. Introduction

Positron emitted inside the human body can either annihilate directly with one of the electrons of the examined organism or it creates the metastable state of electron and positron called positronium (Ps). Positronium may be trapped inside free volumes between and within molecules of the examined patient. Currently, in the commercial PET technique, the phenomenon of positronium production is neither recorded nor used for imaging.

Imaging of the properties of positronium inside the body may deliver new diagnostic information. The average lifetime of positronium depends on the size of the free volumes between atoms (Schrader and Jean, 1988, Coleman, 2000, Tao, 1972, Eldrup et al., 1981) and there are indications (Jasińska et al., 2017b,a, Pietrzak et al., 2013, Liu et al., 2007) that it is correlated with the stage of the development of metabolic disorders of the human tissues. Therefore, an image of the average lifetime and production probability of the positronium formed inside the human body during the routine PET imaging (Moskal et al., 2013), as well as the fraction of its annihilations into three-photons (Kacperski and Spyrou, 2005, Jasińska and Moskal, 2017) may deliver information complementary to the standardized uptake value (SUV) and useful for the diagnosis. In this article we explore a possibility

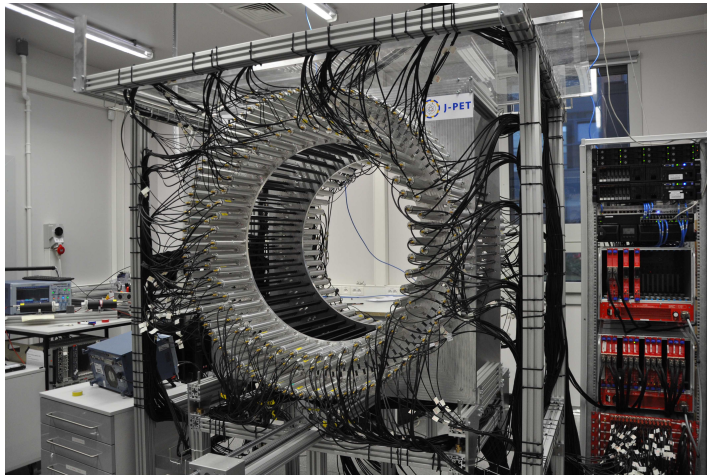


Figure 1: Photo of the prototype of the Jagiellonian Positron Emission Tomograph (J-PET) scanner. The J-PET scanner is built from strips of plastic scintillator with dimensions of $7 \times 19 \times 500 \text{ mm}^3$, forming cylindrical layers (Niedźwiecki et al., 2017, Moskal et al., 2015, 2014) with the inner diameter of 85 cm and the axial field-of-view (AFOV) of 50 cm. Light signals from each strip are converted to electrical signals by Hamamatsu R9800 vacuum tube photomultipliers placed at opposite ends of each strip. Note that the present J-PET prototype consists of 192 scintillator strips only, with empty spaces between the scintillators.

of positronium average lifetime imaging with the J-PET tomograph constructed from plastic scintillators (Moskal et al., 2016, Niedźwiecki et al., 2017). We concentrate on the decay of the ortho-positronium (o-Ps) into three photons and applications of radiopharmaceuticals emitting prompt gamma.

In more than 40% cases, the electron-positron annihilation proceeds in the tissue via creation of positronium (Harpen, 2004, Jasińska et al., 2017b) and even in water the ortho-positronium is formed with the probability of about 25% (Stepanov et al., 2010). Ortho-positronium decays in vacuum into three photons, however, in the human body, due to the large probability of the pick-off processes (Garwin, 1953a), the three-photon events (both from ortho-positronium decays and direct $e^+e^- \rightarrow 3\gamma$ processes) constitute altogether only about 0.5% of electron-positron annihilations (Jasińska et al., 2017b, Jasińska and Moskal, 2017). However, such a relatively low fraction of three-photon annihilations occurring in the human tissues may be compensated by increased detection efficiency of the PET detector and by improved spatial resolution of the single-event annihilation point reconstruction (Gajos et al., 2016, Kacperski and Spyrou, 2005). At present, PET tomographs record and use for image reconstruction less than 1% of annihilation events occurring in the body (Cherry, Badawi, Karp, Moses, Price and Jones, 2017, Cherry, Jones, Karp, Qi, Moses and Badawi, 2017). In this context it is important to emphasize that there is an ongoing development of novel modalities for the whole and total-body PET imaging which shall be characterized by about 40 times higher sensitivity (Viswanath et al., 2017, Zhang et al., 2017, Cherry, Badawi, Karp, Moses, Price and Jones, 2017, Cherry, Jones, Karp, Qi, Moses and Badawi, 2017) with respect to the presently available PET systems (Slomka et al., 2016, Vandenberghe et al., 2016). Moreover, additional improvement in the time resolution to 100 ps, combined with the total-body PET, may considerably increase the sensitivity even by a factor of 200 (Cherry, Jones, Karp, Qi, Moses and Badawi, 2017). Therefore, an efficient positronium imaging may become feasible in the nearest future.

The reconstruction of positronium lifetime requires determination of times of its creation and annihilation. These can be achieved when applying radiopharmaceuticals labeled with isotopes as e.g. Scandium-44 which after emission of the positron changes into a daughter nucleus in an excited state (Walczak et al., 2015, Szkliniarz et al., 2015). The daughter nucleus subsequently de-excites through emission of one or several gamma quanta (often referred to as prompt gamma). Thus, as a result of the decay both: e^+ and γ are emitted e.g. via the following process: $^{44}\text{Sc} \rightarrow ^{44}\text{Ca}^* e^+ \nu_e \rightarrow ^{44}\text{Ca} \gamma e^+ \nu_e$, where, ν_e denotes a neutrino whose interaction probability with the patient and detector is negligible.

Recently, applications of radiopharmaceuticals labeled with metallic β^+ emitters as radioisotopes of scandium (^{43}Sc , ^{44}Sc) have rapidly expanded, particularly for oncologic imaging purposes (Hofman et al., 2012, Krajewski et al., 2013, Huclier-Markai et al., 2014, Walczak et al., 2015). For example the ^{44}Sc labeled DOTATATE due to its high binding affinity for the somatostatin receptors can enhance significantly diagnostics quality of neuroendocrine cancers (Singh et al., 2017).

In the current PET imaging the prompt gamma constitutes a source of background since when reacting via Compton effect it may give a signal in the detector which can be misclassified as signal from a 511 keV photon from the electron-positron annihilation. Analogously, in typical clinical PET, positron-electron annihilation to three photons ($e^+e^- \rightarrow 3\gamma$) constitutes a source of unwanted background which is discarded together with the multi-photon events due to the random coincidences and scatterings in the detectors.

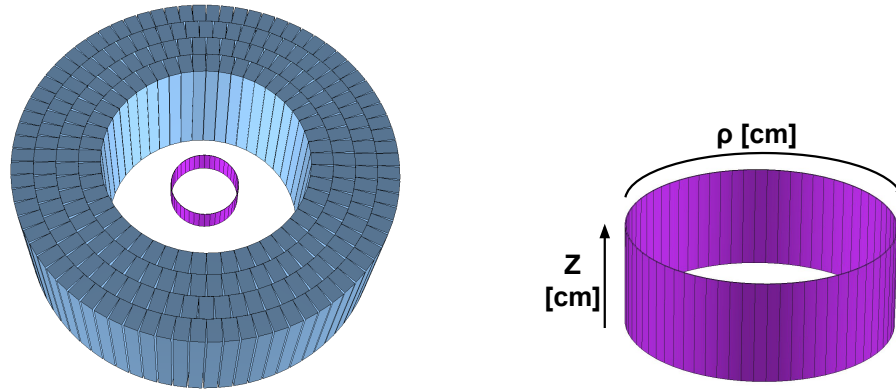


Figure 2: Left: visualization of simulated cylindrical shape detector. Detector consists of four layers and each of them is filled with scintillators. In this article the simulations were performed assuming scintillators dimensions of $7 \times 19 \times 500 \text{ mm}^3$ and the inner layer radius of 43 cm. However, for clarity the elements are shown not to scale. In each layer only a selected number of scintillators with increased x-y dimensions is shown. Inside the detector a cylindrically shaped phantom is placed. Right: visualization of simulated phantom ($R_{inner} = 10.0 \text{ cm}$, $R_{outer} = 10.1 \text{ cm}$, $z = 10.0 \text{ cm}$) with coordinate system as described in the text. The phantom is composed of various materials in which the lifetime of ortho-positronium atoms varies from 2200 ps to 2300 ps as expected for the positronium in the human body. A comprehensive discussion of the known results on o-Ps lifetime can be found in section 2.

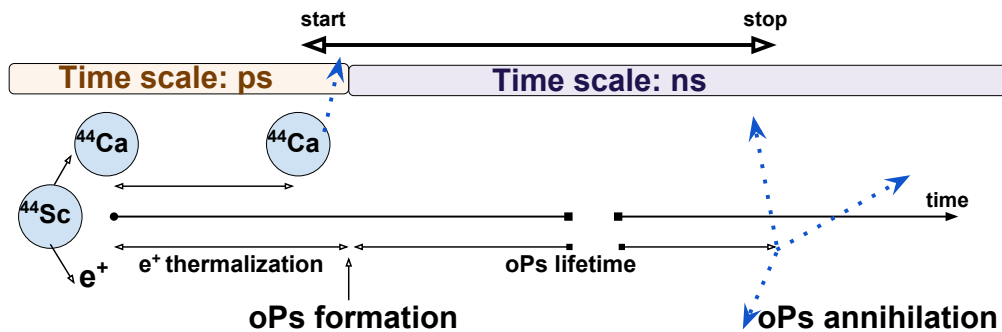


Figure 3: Scheme of scandium β^+ decay that leads to formation of ortho-positronium state. The ^{44}Sc isotope emits a positron which thermalizes in the body and forms an ortho-positronium bound state. Independently, the remaining $^{44}\text{Ca}^*$ nucleus deexcites after a few picoseconds (*NUCLEIDE-LARA - Library for alpha, X and gamma emissions, 2017*) emitting a prompt gamma with characteristic energy. Both the time scale of thermalization (*Schrader and Jean, 1988*) and ^{44}Ca excited state lifetime are in the order of picoseconds, while the lifetime of created ortho-positronium is in the order of nanoseconds. This allows to treat the de-excitation photon emission time as the time when the ortho-positronium was formed. The o-Ps annihilation time is reconstructed based on gamma photons hit-times and hit-positions in the detector.

However, the triple coincidences originating from $e^+e^- \rightarrow 3\gamma$ processes or occurring when utilizing the $\beta^+\gamma$ emitters may be useful for imaging. Since more than a decade, there is also an ongoing research aiming at improvement of spatial resolution of the annihilation point reconstruction when using $\beta^+\gamma$ emitters by combining standard PET tomography technique with the various types of Compton cameras for the registration of the prompt gamma (Lang et al., 2012, 2014, Thirolf et al., 2015, Grignon et al., 2007, Donnard et al., 2012, Oger et al., 2012). Also a fraction of detector scatter coincidences may be applied to improve the image by recovering true Lines of Response (LORs) from triple coincidences (Lin et al., 2016, Cal-González et al., 2015).

Image reconstruction based on the three-photon annihilation was also proposed more than decade ago by (Kacperski et al., 2004, Kacperski and Spyrou, 2005, Abuelhia et al., 2007). The proposed method enables a reconstruction a place of the $e^+e^- \rightarrow 3\gamma$ annihilation based on the measurement of energies of three photons and positions of their interactions in the detector material. The application of energy and momentum conservation laws allows to reconstruct the annihilation point on an event-by-event basis. However, the precise measurement of photon energies requires applications of high-resolution semiconductor detectors (such as e.g. CdZnTe (Kacperski and Spyrou, 2005, Abuelhia et al., 2007)) rendering the implementation of the full scale PET scanner relatively expensive.

In this article we present a cost-effective method enabling reconstruction of the density distribution of the $e^+e^- \rightarrow 3\gamma$ annihilation points, as well as reconstruction of the image of ortho-positronium properties, such as its average lifetime and production probability. The

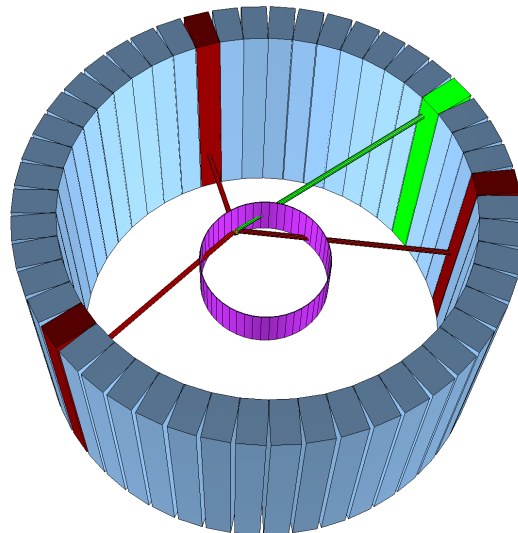


Figure 4: A scheme of a simulated detector and phantom located inside it with an exemplary $e^+e^- \rightarrow 3\gamma$ annihilation event. For clarity only a single layer of detector is shown with decreased number of scintillators and increased x-y dimensions. Red lines represent the photons originating from ortho-positronium annihilation, while green line shows prompt gamma originating from β^+ emitter de-excitation, e.g. from $^{44}\text{Sc} \rightarrow ^{44}\text{Ca}^* e^+ \nu \rightarrow ^{44}\text{Ca} \gamma e^+ \nu$ decay chain. Photon recording strips are marked with corresponding colors.

proposed imaging of ortho-positronium properties produced in the living organism is based on the time of signals registered with the plastic scintillators (Moskal et al., 2013). Thus, the precision of the proposed method relies predominantly on the time resolution of the tomograph since the measurement of energy losses of registered photons is used only to disentangle signals between prompt gamma and annihilation photons. The measured times are used to reconstruct the hit-times and hit-positions of registered photons which enables the reconstruction of the time and position of the annihilation point. A prototype of the tomograph enabling application of this method has been built (Fig. 1) (Niedźwiecki et al., 2017, Dulski et al., 2018) and validated for classical PET imaging (Pawlik-Niedźwiecka et al., 2017).

Here we explore the possibility of performing positronium imaging using dedicated Monte-Carlo simulation procedures which are described in detail in references (Kamińska et al., 2016, Gajos et al., 2016). The simulations are carried out assuming an ideal case, that the tomograph is built from four concentric layers of axially arranged plastics scintillator strips adjacent to each other as indicated in Fig. 2, left panel.

In order to reconstruct a mean lifetime of ortho-positronium atoms in each voxel of the patient it is necessary to determine the times of the ortho-positronium creation and decay (see Figure 3). The scheme of the detector with recorded o-Ps $\rightarrow 3\gamma$ annihilation is shown in Figure 4. The time of creation is determined using the prompt gamma e.g. from ^{44}Sc , since nuclear deexcitation is much faster (few picoseconds) than positronium lifetime.

The annihilation point and time of $e^+e^- \rightarrow 3\gamma$ processes is reconstructed in an analytical way based on the measured times and positions of the three photons (X_i, Y_i, Z_i, T_i) , $i = 1, 2, 3$ and knowing that (due to the momentum conservation principle) all three photons momentum vectors and the annihilation point (x, y, z) are lying in a single plane, referred to as the decay plane (Gajos et al., 2016). Co-planarity of the 3γ reduces the reconstruction to a two dimensional problem of three equations: $(T_i - t)^2 c^2 = (X'_i - x')^2 + (Y'_i - y')^2$, where X'_i, Y'_i, T_i (for $i=1, 2, 3$) denote hit-coordinates and hit-times in the decay plane reference system, x', y', t denote the annihilation point's coordinates and time in this frame, and c stands for the speed of light. Solving this system of three equations defined for $i = 1, 2, 3$ yields the time and location point of the $e^+e^- \rightarrow 3\gamma$ annihilation.

Table 1: Selected physical characteristics of the exemplary beta-plus isotopes use for both: PET imaging and positron annihilation lifetime spectroscopy (PALS) investigations. Data were adapted from *National Nuclear Data Center* (2016).

Isotope	Half-life	β^+ decay	E_γ [MeV]	Excited nuclei lifetime
^{44}Sc	4.0 h	$^{44}\text{Sc} \rightarrow ^{44}\text{Ca} + e^+ + \nu_e + \gamma$	1.16	2.61 ps
^{14}O	70.6 s	$^{14}\text{O} \rightarrow ^{14}\text{N} + e^+ + \nu_e + \gamma$	2.31	67.8 fs

The registration of the prompt gamma, in addition to the annihilation photons, permits to measure the differences between the time of formation and the time of annihilation of positronium on the event-by-event basis (Moskal et al., 2013, Gajos et al., 2016, Kamińska et al., 2016). Reconstructed time of the prompt gamma emission is used as the formation

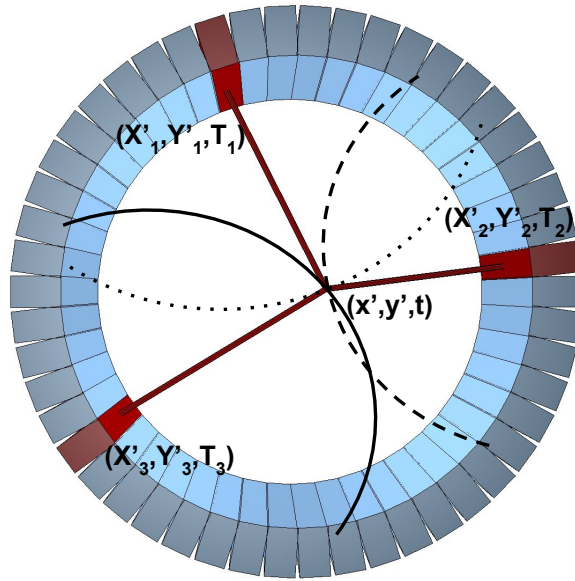


Figure 5: A scheme of the detector showing $o\text{-Ps} \rightarrow 3\gamma$ annihilation. For clarity only a single layer with registered hits is shown. Red lines represent the gamma photons from ortho-positronium annihilation. Figure shows a single layer of the detector in 3D view with cross-section of the scintillators shown in grey and their inner side in blue. The trilateration method is used to determine the annihilation position and time (x', y', t) along the annihilation plane. For each recorded photon a circle, which is a set of possible photon origin points, centered in the hit-position and parameterised with the unknown $o\text{-Ps}$ annihilation time is considered. The intersection of the three circles corresponds to the $o\text{-Ps} \rightarrow 3\gamma$ annihilation point.

time of the positronium. This approximation leads to negligible uncertainties, since the time between the emission of the positron and the formation of the positronium, as well as the average lifetime of the excited nuclei relevant for PET examinations (e.g. $^{44}\text{Ca}^*$), are both in the order of a few picoseconds (see Table 1).

Finally, it is worth to note that if the time resolution would be improved in the future down to 10 ps, as advocated by Lecoq (2017), then 2γ pick-off annihilations may be used to determine the annihilation time and position for each event, which in coincidence with the registration of prompt gamma would allow to determine lifetime spectra for each voxel and, hence, to reconstruct the ortho-positronium lifetime based on $o\text{-Ps} \rightarrow 2\gamma$ pick-off annihilations. Such ortho-positronium pick-off annihilations for the human body (with the $o\text{-Ps}$ lifetime of about $\tau_{\text{tissue}} \sim 2$ ns) are about 70 times $(\frac{\tau_{\text{vacuum}}}{\tau_{\text{tissue}}} - 1)$ more frequent than $o\text{-Ps} \rightarrow 3\gamma$ events. Therefore, the proposed method of positronium imaging shall become practical with the advent of total-body PET and improved time resolutions.

The article is organized as follows: In section 2 the positronium properties in vacuum and in the human body are briefly reviewed based on the performed experiments up to date. This section concludes with the estimation of the range and values of lifetimes of ortho-positronia produced in the various tissues of the human body (~ 1.8 ns – ~ 2.5 ns), as well as in the expected differences in the ortho-positronium lifetime between the healthy and

cancerous tissues (~ 50 ps – ~ 200 ps). The section 3.1 contains a general description of the J-PET detector in order to illustrate the possibility of applying the introduced method for the ortho-positronium lifetime imaging simultaneously to the regular PET scan. This section defines also the properties of the detection system for which the feasibility study of the positronium imaging will be performed in Section 3.3. The description of the Monte Carlo simulation given in section 3.3 comprises: (i) description of the four-layer detector built from axially arranged plastic strips adjacent to each other, (ii) three-photon annihilation as predicted by the theory of quantum electrodynamics, (iii) gamma photon interaction within detector build from plastic scintillators as a function of incident gamma photon energy, (iv) resolution for reconstructing position, time and energy loss of gamma photons in the detector, (v) reconstruction of annihilation position based on the reconstructed gamma photon hit information. Next, Section 4 includes details on positronium mean lifetime image reconstruction, discussion about the achievable mean-lifetime resolution and positronium imaging sensitivity.

2. Positronium in the human body

Similarly to the hydrogen atoms, positronium may be formed in a singlet or triplet spin states, referred to as para-positronium and ortho-positronium, respectively. Due to the charge conjugation symmetry conservation, the para-positronium annihilates with emission of an even number of photons and ortho-positronium annihilation is subject to emission of an odd number of photons. Predominantly these are two and three photons for para- and ortho-positronium atoms, respectively. The decay time of formed positronium depends on its quantum state: the observed lifetime for para-positronium localized in vacuum amounts to ~ 125 ps, while, due to the smallness of the fine structure constant and the phase-space volume available, in the decays of the ortho-positronium its lifetime in vacuum is three orders of magnitude greater ($\tau_{vac.} = 142$ ns) (Al-Ramadhan and Gidley, 1994, Vallery et al., 2003, Jinnouchi et al., 2003). When formed inside matter, positronium may be trapped inside volumes of lower electron density. However, the positronium trapped in a free volume is susceptible to the pick-off processes (Garwin, 1953b), in which positron from the positronium may annihilate with one of the surroundings electrons. The smaller are the free voids between the atoms the larger is the probability of the pick-off process and, hence, the smaller is the mean lifetime of the trapped positronium. This effect is significant in case of ortho-positronium for which the mean lifetime may change in the range from about 142 ns to even below 1 ns. The correlation is described in the framework of well tested models which relate quantitatively the mean ortho-positronium lifetime with the size of the free void in the range from 0.2 nm up to 100 nm (Tao, 1972, Eldrup et al., 1981, Goworek et al., 1997, 1998). In addition it is well known from the Positron Annihilation Lifetime Spectroscopy (PALS) studies that the intensity of the production of ortho-positronium atoms is strongly correlated with the free voids size distributions and their concentration (Goworek et al., 1982, Kobayashi et al., 1989, Schrader and Jean, 1988, Coleman, 2000, Jasińska and Dawidowicz, 2003, Jasinska et al., 2003).

In the human body, positronium atoms can be created and trapped both, in the dense tissue and in the bio-fluids - importantly, including water. In purified water the o-Ps lifetime amounts to 1.8 ns and its production probability is equal to about 25% (Stepanov et al., 2011). There are few works demonstrating the application of PALS technique to model and living biological systems reporting differences between normal and cancerous cells and changes of the o-Ps lifetime during dynamical processes undergoing in cells (Jean and Ache, 1977, Liu et al., 2007, Jean et al., 2006, 2007, Liu et al., 2008, Yas et al., 2012, Axpe et al., 2014, Kubicz et al., 2015). Recently, significant differences in PALS parameters between normal and diseased tissues were also observed in samples of uterine leiomyomiasis and normal muscles tissues taken from women-patients after surgery of uterus tumors (Jasińska et al., 2017b,a). The results of above quoted research indicate that in all investigations performed to date there is a difference in PALS parameters determined for healthy and cancerous tissues. Thus, as suggested in references (Moskal et al., 2013, Jasińska and Moskal, 2017), measurements of properties of ortho-positronium atoms (such as lifetime and production probability, or $3\gamma/2\gamma$ rate ratio) which are formed inside the human body during a routine PET imaging may deliver information useful for the diagnostics. In this article as a first step on a way towards realisation of such measurements, we present a feasibility study of the reconstruction method of the image of ortho-positronium lifetime proposed in reference Moskal et al. (2013).

The mean ortho-positronium lifetimes in the tissues varies from about 1.8 ns (as in pure water) to about 2.5 ns (or even up to about 4 ns as measured for the human skin with low energy positron beam (Chen et al., 2012)). Whereas, the mean ortho-positronium lifetime differences for healthy and cancerous tissues are in the range of about 50 ps to about 200 ps (Jasińska et al., 2017b, Pietrzak et al., 2013, Liu et al., 2007).

Taking into account the above information, the feasibility study of the positronium lifetime imaging will be performed assuming the formations of ortho-positronium atoms in a set of point-like sources and in a virtual phantom formed from tissues in which ortho-positronium lifetime varies from 2.0 ns to 3.0 ns. The phantom will be inserted into an idealized version of the J-PET tomograph consisting of four cylindrical layers. In the simulations the properties of the detection system, which are briefly described in the following section, will be taken into account.

3. Materials and methods

3.1. Principles of operation of the J-PET detector made of plastic scintillators

The J-PET tomograph (shown in Fig. 1) is a cylindrically shaped PET detector made of plastic scintillators. The light signals are converted to electric pulses by photomultipliers connected optically at the two ends of a scintillator. In plastic scintillators, which are composed of elements of low atomic number, incident photon interacts mainly through the Compton scattering leading to a continuous energy loss distribution. Fig. 6 presents an example of the energy loss spectra for photons from $e^+e^- \rightarrow 2\gamma$ annihilation and for prompt gamma from ^{44}Sc and ^{14}O .

In the J-PET tomograph the electric signals from photomultipliers are processed by the front-end electronics based on Field Programmable Gate Arrays (FPGA) (Pałka et al., 2017), collected by means of the triggerless data acquisition system (Korcył et al., 2016, 2018), and analysed using a dedicated analysis software framework (Krzemień et al., 2015).

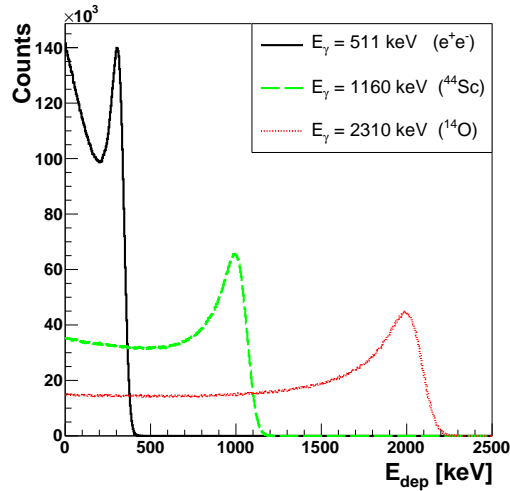


Figure 6: Simulated energy loss spectra for annihilation photons (511 keV) and prompt gamma from the decay of isotopes indicated in the legend. The shown distributions include the energy resolution of the J-PET detector (Moskal et al., 2014).

The uncertainty of the hit-time determination and hence the Time-Of-Flight (TOF) resolution depends on the length of the scintillator strip and the Coincidence Resolving Time (CRT) varies from $\text{CRT} \approx 0.230$ ns to $\text{CRT} \approx 0.440$ ns when the length changes from 15 cm to 100 cm (Moskal et al., 2016), and it may be improved by using a matrix of silicon photomultiplier (SiPM) readout. In Reference Moskal et al. (2016) it was shown that e.g. for the 2×5 SiPM matrix at two ends of the scintillator strip the coincidence resolving time changes from $\text{CRT} \approx 0.170$ ns to $\text{CRT} \approx 0.365$ ns when extending an axial field-of-view (AFOV) from 15 cm to 100 cm (Moskal et al., 2016).

It is worth emphasizing that even higher time resolution of $\text{CRT} = 0.100$ ns was already achieved with the small $3 \times 3 \times 5$ mm³ LaBr₃:Ce(5%) crystals read out with the SiPMs (Schaart et al., 2010). More recently a detector design with SiPM has been reported, with $\text{CRT} = 0.085$ ns for $2 \times 2 \times 3$ mm³ LSO:Ce codoped 0.4%Ca crystals and CRT of 0.140 ns for $2 \times 2 \times 20$ mm³ crystals with the length as used in the current PET tomographs (Nemallapudi et al., 2015). Therefore, in section 3.3 we will perform feasibility studies simulating the possibility of positronium imaging under conservative assumption that CRT is equal to 0.140 ns, as already achieved for the solutions applicable in the current PET detectors.

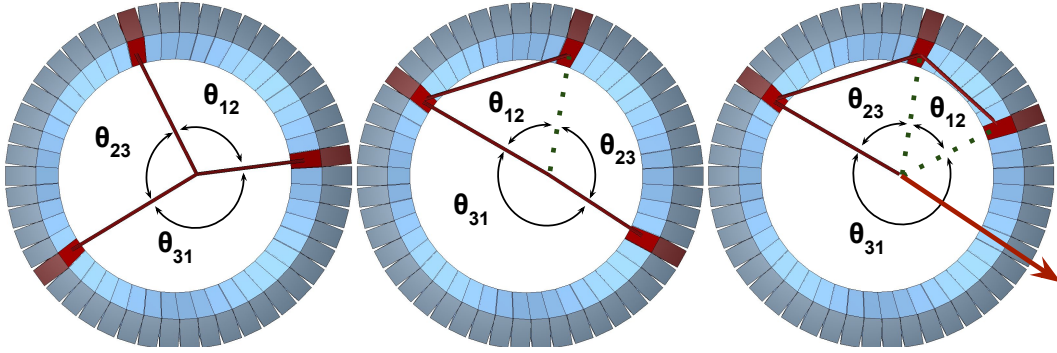


Figure 7: Typical topology of $o\text{-Ps} \rightarrow 3\gamma$ (left panel) and background events originating from 2γ annihilations (middle and right panels). Red solid lines denote actual photons, the red arrow indicates not registered photon while green dotted lines indicate reconstructed photon candidates. The numbering of photons is such that $\theta_{12} < \theta_{23} < \theta_{31}$.

3.2. Event selection criteria and background reduction

An event useful for reconstruction of the $o\text{-Ps}$ image is shown pictorially in Fig. 4. It consists of four registered gamma interaction points in the scintillator strips (later on referred to as *hits*), three of them originating from the $o\text{-Ps} \rightarrow 3\gamma$ annihilation and the fourth one from the prompt gamma. After identification of the prompt gamma (e.g. using energy loss criterion $E_{dep} > 370$ keV), the three remaining hits with $E_{dep} < 370$ keV become then candidates of photons originating from the $o\text{-Ps} \rightarrow 3\gamma$ decays useful for the reconstruction of annihilation position and time as indicated in Fig. 5. However, due to the secondary Compton scattering in plastic scintillator (discussed in more detail in references (Kowalski et al., 2015, 2016, 2018, Kamińska et al., 2016)), the 2γ events may mimic registration of 3γ ones, as indicated pictorially in Figure 7. Yet, we can disentangle true and false 3γ events based on the (i) relation between hit positions and hit times and (ii) angular correlation of relative angles between the direction of annihilation photons.

For example, events for which both photons from $e^+e^- \rightarrow 2\gamma$ annihilation are registered and one of them is scattered causing signals in two detectors (middle panel of Fig. 7) satisfy the condition $\theta_{12} + \theta_{23} = 180^\circ$ and are concentrated along the anti-diagonal of the θ_{12} vs. θ_{23} plot. Detailed studies were done in Ref. Kamińska et al. (2016) and show that the application of the angular correlation criterion suppresses the background from 2γ by the factor of about 10^4 while rejecting only 3% of true 3γ signal events and that further requirements based on the relation between hit position and hit time may reduce the background by another few orders of magnitude.

Therefore, even though the 3γ events are expected to constitute only about 0.5 % of 2γ events, the background due to the 2γ annihilation associated with the secondary scattering in the detector can be reduced to a negligible level. Hence, in the next section we present simulations assuming that the hits from the $o\text{-Ps} \rightarrow 3\gamma$ annihilation can be identified and we will focus on the possibilities of the positronium lifetime image reconstruction, assuming that the time resolution of the detector amounts to $\text{CRT} = 0.140$ ns.

3.3. Monte Carlo simulations

The feasibility studies of positronium imaging are performed based on the virtual cylindrical phantom placed inside the J-PET tomograph as shown in Fig. 2. A cylindrically shaped phantom with radii of $R_{inner} = 10.0$ cm, $R_{outer} = 10.1$ cm and $z = 10.0$ cm is placed along the z axis of the detector (see Figure 2, right panel). The volume of the phantom was divided into 2 parts, each corresponding to the tissues characterized with different average lifetimes of ortho-positronium atoms. The values of average lifetimes of 2200 ps to 2300 ps were chosen. These values are within the range of lifetimes expected for the ortho-positronium in the human body (as discussed in sections 1 and 2).

For the studies presented in this article about 3×10^9 events of o-Ps decays into three photons were generated and, subsequently, the response of the J-PET tomograph was simulated and then the image of the mean lifetime of positronium was reconstructed. The simulations were conducted in the following steps: For each event (i) the position of the annihilation was generated, assuming a homogeneous density distribution within the cylindrical phantom; (ii) the lifetime of a given o-Ps atom was generated with the exponential probability density distribution with the mean lifetime depending on the position in the phantom; (iii) the momentum vectors of photons from the o-Ps $\rightarrow 3\gamma$ decay were generated according to the predictions of the Quantum Electrodynamics ‡; (iv) hit-position and energy deposition of each photon in the plastic scintillators of the J-PET tomograph were simulated taking into account the cross sections for the Compton interactions of gamma photons in the plastic scintillators; (v) the experimental resolutions for the registration of time and position of gamma photons were accounted for by smearing the values of generated hit-times and hit-positions with the resolution functions of J-PET, assuming the CRT value of 0.140 ns; (vi) for each *registered* event, a time and position of o-Ps annihilation was reconstructed using the trilateration method (Gajos et al., 2016) and the image of mean o-Ps lifetime was created. The simulation methods for the above listed steps from (i) to (v) were described in details in the previous publications (Moskal et al., 2016, Kamińska et al., 2016, Moskal et al., 2014, 2015).

At the step of generation of the position of annihilation and the decay time of o-Ps in the phantom, the area of the phantom was divided into pixels with dimensions of 2 cm \times 2 cm. The generated mean lifetime distribution as a function of the $z - \rho$ coordinates along the cylinder is shown in Figure 8. A colour code indicates the mean life-time of o-Ps calculated in each pixel, using lifetime values of ortho-positronium atoms generated in the pixel. The differences in the mean lifetimes observed within each of two sections are due to the finite statistics of generated events. Thus, Figure 8 presents an image of o-Ps mean lifetimes which could be reconstructed in the case of an ideal detector, assuming that all of the annihilations events were registered with an ideal resolution.

In addition, we preformed a simulation positioning six point annihilation sources in the arrangement required by the National Electrical Manufacturers Association (NEMA, 2012)

‡ The positronium has a small boost along the initial positron momentum. Due to this the annihilation photons' momenta slightly deviate from co-planarity in the detector frame of reference. This effect is included in the simulations and its contribution is negligible with respect to the resolution achieved so far (Gajos et al., 2016).

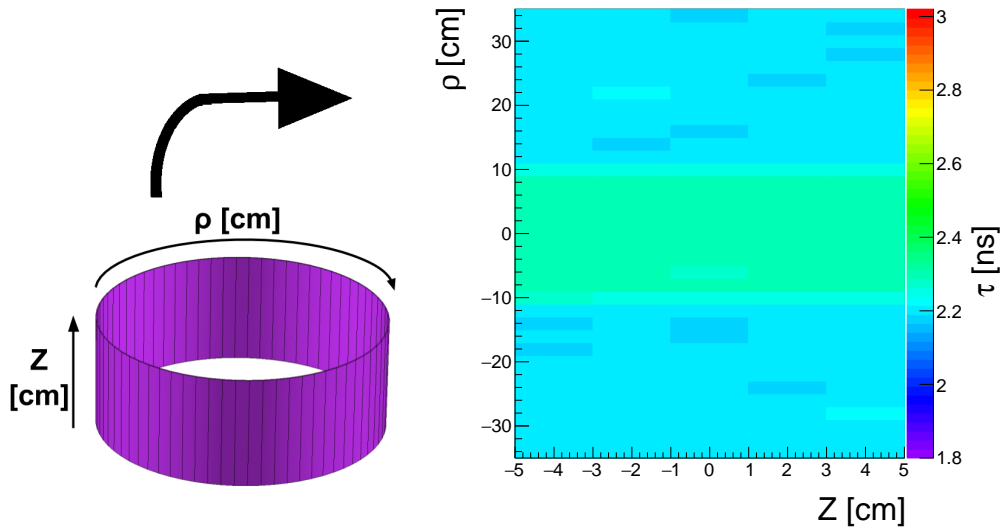


Figure 8: Generated distribution of mean ortho-positronium lifetime in the phantom as a function of z and ρ coordinates. Pixel size is $2 \text{ cm} \times 2 \text{ cm}$. Radiopharmaceutical is uniformly distributed, however the phantom is composed of two different materials in which the lifetime of ortho-positronium atoms is equal to 2300 ps (green area) and 2200 ps (blue area).

norm: a six sources (cylinders $r = 0.5 \text{ mm}$, $z = 1 \text{ mm}$) were placed as presented in Table 2. Simulations included response of the detector using time and position resolutions as discussed in the text of the article.

Table 2: Coordinates of simulated "point-like" sources positioned according to the NEMA norm. Each source is characterized by a different o-Ps lifetime.

Position	Coordinates [cm]	Simulated o-Ps lifetime [ns]
1	(1,0, 0)	2.0
2	(10,0, 0)	2.4
3	(20,0, 0)	2.8
4	(1,0, 18.75)	2.2
5	(10,0, 18.75)	2.6
6	(20,0, 18.75)	3.0

4. Results

As a result of simulated measurements and data selection described in the previous sections for each registered o-Ps $\rightarrow 3\gamma$ event a hit-time and hit-position of the annihilation and deexcitation photons are determined. For each event these enable a reconstruction of time and position of the annihilation point using the trilateration method (Gajos et al., 2016), as well

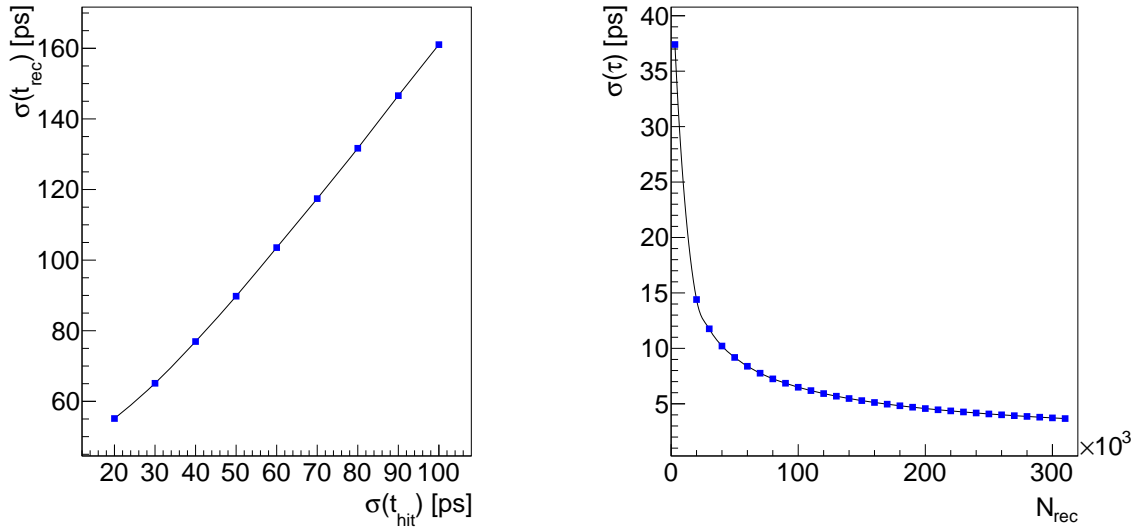


Figure 9: Left: Resolution of ortho-positronium reconstructed decay time obtained by the trilateration method as a function of detector time resolution. Achievable resolution strongly depends on detector timing capabilities. Right: Resolution of the mean lifetime determination as a function of detected entries in a single voxel. An example for $\sigma(t_{\text{hit}}) = 40$ ps (corresponding to CRT ≈ 140 ps) and $\tau = 2010$ ps is presented.

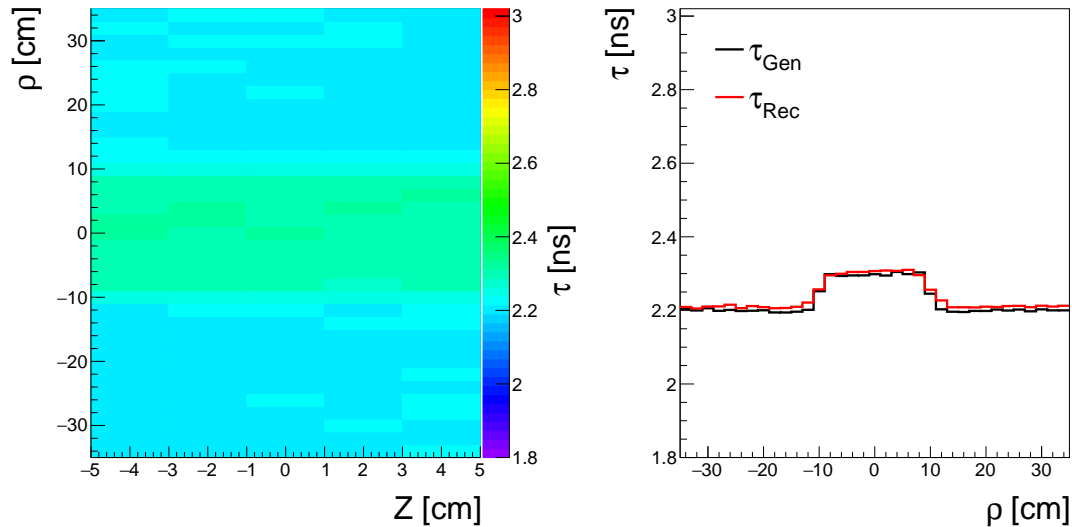
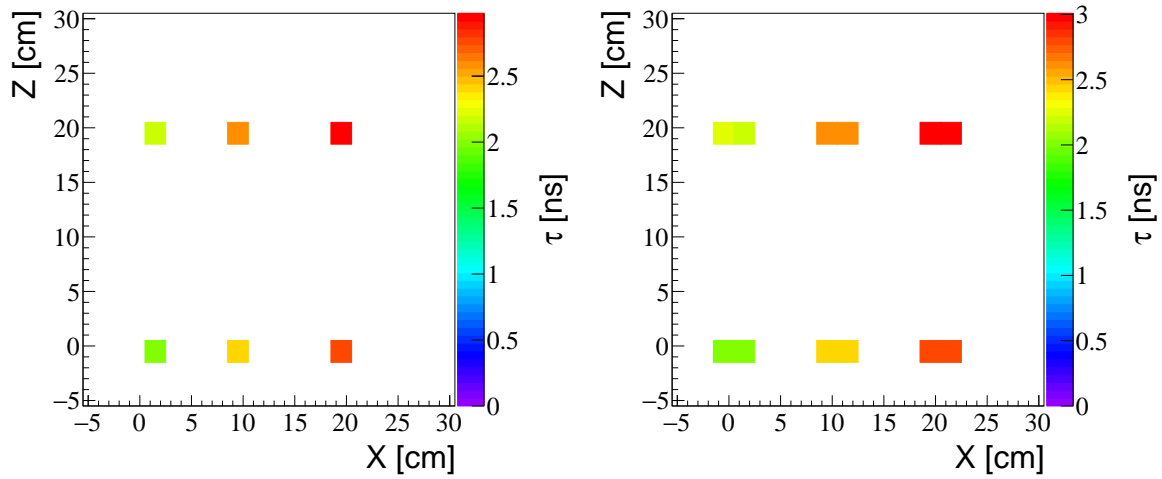
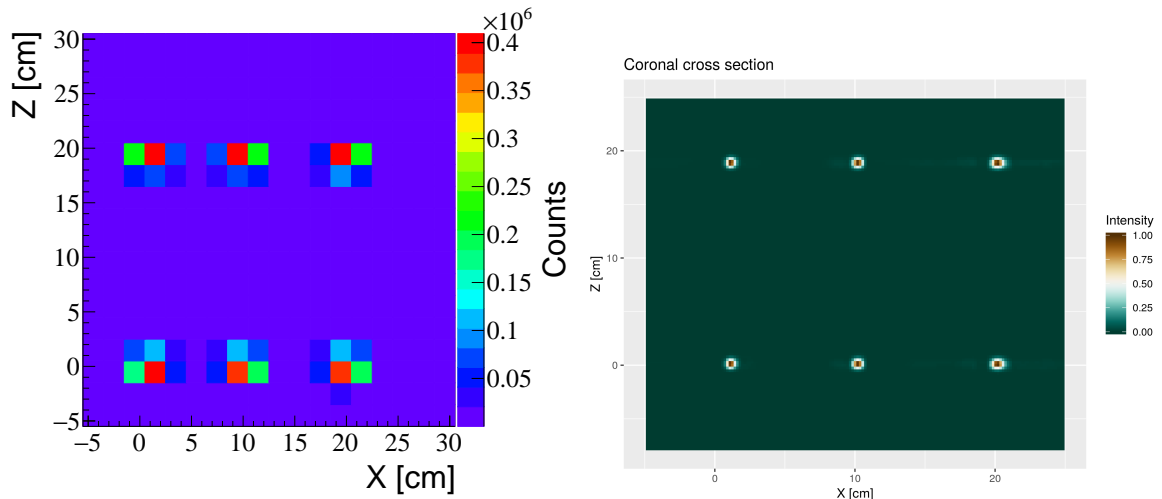


Figure 10: Left: Reconstructed image of the phantom composed of two materials in which the lifetime of ortho-positronium atoms is equal to 2200 ps (blue area) and 2300 ps (green area). Generated image is shown in Figure 8. The o-Ps annihilation time is reconstructed by using the trilateration method and assuming time resolution of $\sigma(t_{\text{hit}}) = 40$ ps corresponding to CRT of about 140 ps, as discussed in the introduction. Right: Comparison between generated (black line) and reconstructed (red line) o-Ps lifetime image shown as a function of transverse radius.



(a) Generated ortho-positronium lifetime distribution. (b) Reconstructed ortho-positronium lifetime distribution.



(c) Reconstructed distribution of annihilation point spatial coordinates. (d) Reconstructed image of six sources obtained while applying the Filter Back Projection algorithm for 2γ events.

Figure 11: A six point sources were placed according to the positions denoted in Table 2. Each source has a different ortho-positronium lifetime (a). Application of 3γ trilateration-based algorithm (Gajos et al., 2016) allows to reconstruct distribution of spatial coordinates of annihilation points (c) as well as the mean lifetime distribution of the ortho-positronium (b). The voxel size is equal to $2\text{ cm} \times 2\text{ cm} \times 2\text{ cm}$. For comparison result of standard PET imaging for 2γ events is shown (d).

as the lifetime of ortho-positronium estimated as a difference between the emission time of annihilation photons and emission time of the prompt gamma. For the purpose of positronium mean-lifetime image reconstruction an object is divided into voxels in which $o\text{-Ps} \rightarrow 3\gamma$ annihilations are recorded. In each voxel the mean lifetime is estimated by the arithmetic mean of individual lifetimes. Reconstruction time-resolution of a single ortho-positronium lifetime strongly depends on detector timing capabilities (see left panel of Figure 9) while the resolution of mean lifetime determination depends additionally on the number of detected events (see right panel of Figure 9). The mean-lifetime resolution of about 40 ps is achievable for about 3000 events per voxel.

The left panel of Figure 10 shows the image of positronium lifetime reconstructed, assuming the CRT of 140 ps (corresponding to $\sigma(t_{hit})$ of about 40 ps). The original (ideal) image is shown in Figure 8. The reconstructed mean lifetime image (Figure 10) indicates, that for CRT of about 140 ps the method allows to distinguish between o-Ps lifetime differing by 100 ps. Right panel of Figure 10 compares projections of the generated and simulated images. It indicates that the reconstructed positronium lifetime image is in a very good agreement with the generated one. The achieved time resolution for positronium mean lifetime includes also uncertainties due to the depth of interaction (which can be estimated to about 70 ps per event (Moskal et al., 2016)). There is still a room for the future improvement of both the time resolution and accuracy of DOI determination (see e.g. (Lecoq, 2017, van Dam et al., 2011, Pizzichemi et al., 2016)).

Results of the test of the discussed image reconstruction method on the "point-like" sources arranged according to the NEMA norm is presented in Figure 11. In Figure 11 the coronal (XZ) cross-section along $y = 0$ cm is shown, for all six positions of the source. In each source a different o-Ps lifetime were assumed (see Table 2). Reconstructed and generated ortho-positronium lifetime are in agreement (compare Figure 11a and 11b). Spread originates from uncertainty of the reconstructed spatial coordinates of the annihilation point.

The conventional PET imaging on simulated 2γ events (see Figure 11d) and trilateration-based reconstruction of ortho-positronium decays into 3γ photons (see Figure 11c) were performed. The Filtered Back Projection (FBP) is a standard approved by NEMA for the estimation of spatial resolution. Therefore, we employed 3D Reprojection (3DRP) FBP algorithm for image reconstruction, implemented in STIR framework (Thielemans et al., 2012). STIR does not support multilayer geometry, hence all events were remapped onto a single layer of radius $R = 43.73$ mm, comprising the same 7-mm wide strips, 384 in total (an ideal scanner, defined in previous works (Shopa et al., 2017)). After the smearing of times and Z -positions of hits were applied, a SAFIR package was utilised (Becker et al., 2017) for data conversion from list-mode into a STIR-compatible format. In Figure 11d, the coronal (XZ) cross-section along $y = 0$ cm is shown, for all six positions of the source, aggregated into one image. It is important to note that transverse spatial resolution is expected to be higher for the initial 4-layer scanner, since it provides better sinogram sampling in projection space.

The efficiencies for the registration of three photons from the $o\text{-Ps} \rightarrow 3\gamma$ annihilation with the four-layer J-PET with AFOV of 50 cm and 200 cm are shown in the Fig. 12. The

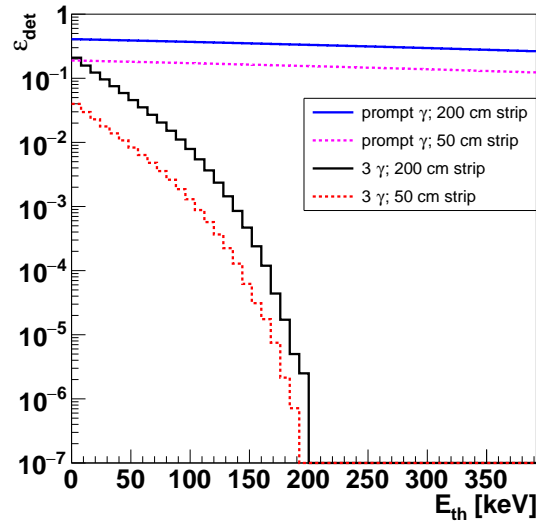


Figure 12: Registration efficiency for prompt gamma (upper lines) and $o\text{-Ps} \rightarrow 3\gamma$ as a function of the energy-loss threshold (determined at the center of the tomograph, taking into account geometrical acceptance, probability of gamma photons registration in the plastic scintillator and J-PET detector resolution). The dashed and solid lines indicate efficiencies for 50 cm and 200 cm strip length, respectively.

efficiencies are plotted as a function of the energy loss threshold. For the threshold of 25 keV the determined efficiency for $o\text{-Ps} \rightarrow 3\gamma$ amounts to 2% and 9% for AFOV of 50 cm and 200 cm, respectively. Thus, about 2×10^8 3γ events can be collected assuming that: (i) activity of 370 MBq (10 mCi) is administered to the patient (Cherry, Jones, Karp, Qi, Moses and Badawi, 2017), (ii) the data is acquired during 20 minutes according to the standard total body protocol, (iii) the sensitivity for 3γ detection with total-body J-PET amounts to 9%, (iv) the fraction of 3γ annihilations is equal to 0.5%.

In addition, taking into account the sensitivity for the detection and selection (energy loss larger than 370 keV) of the prompt gamma equal to about 27% (blue solid line in the right panel of Figure 12), one obtains 5×10^7 registered 3γ events in coincidence with the prompt gamma. This gives a promising perspective, especially in view of the recent works showing that for the current PET with AFOV = 25.5 cm (Siemens mMR PET/MR scanner) even 10^6 counts in the scan could be sufficient to provide good images (Yan et al., 2016). 5×10^7 registered events result in, on average, about 700 events per cubic centimeter of the examined patient. However, the effective imaging sensitivity may be significantly enhanced by improving spatial resolution of the determination of the annihilation position for a single event. The signal-to-noise ratio (SNR) in the conventional PET image is proportional to the square root of sensitivity S , $SNR \sim \sqrt{S}$, and it may be increased effectively by improving the uncertainty in the localization of the annihilation point ΔX ($SNR \sim \sqrt{1/\Delta X}$) (Conti, 2009, Eriksson and Conti, 2015), where ΔX is proportional to the time resolution (e.g. CRT = 0.5 ns gives $\Delta X = 7.5$ cm). For the activity distributed homogeneously in 40 cm diameter phantom

the SNR increases with $\Delta X = 7.5$ cm by a factor of about 2.3 (Townsend, 2008), corresponding to the effective sensitivity growth by a factor of about 5.3. Thus, improving ΔX to 1 cm would lead to a gain in sensitivity by a factor of about 40 with respect to non-TOF PET systems. The three photon iterative image reconstruction methods remains to be elaborated, nevertheless, this challenge is far beyond the scope of this article. Thus, presently, in the case of the three photon reconstruction discussed in this article, it is impossible to precisely evaluate the gain in effective sensitivity due to the improvement of the spatial resolution of annihilation point reconstruction. However, the estimations of the sensitivity of about 9% for three photon registration with the 200 cm long J-PET, and the estimated spatial resolution for a single event of about 1 cm (Gajos et al., 2016) give promising perspectives for the future application of the positronium imaging even though the fraction of three photons annihilations in human body is expected to be at the level of about 0.5 % only.

5. Summary and perspectives

In this article we presented a cost-effective method enabling reconstruction of the density distribution of the $e^+e^- \rightarrow 3\gamma$ annihilation points, as well as reconstruction of the image of ortho-positronium average lifetime. The proposed method is based on the time of signals registered with plastic scintillators and its precision relies predominantly on the time resolution of the tomograph. The arrival times of signals measured at the ends of scintillator strips are used to reconstruct the hit-times and hit-positions of registered gamma photons. Next, the annihilation point is reconstructed analytically, on an event by event basis, using trilateration method and taking advantage of the fact that all three photons from the decay of ortho-positronium are lying in single plane.

We explored the possibility to apply the introduced method for the reconstruction of images of mean lifetime of ortho-positronium which are created in patients body during the routing PET investigations. In the patient about 40% of e^+e^- annihilations proceed via formation of positronium atoms with about 0.5% decaying into 3γ (Harpen, 2004, Jasińska et al., 2017b). Though the relative rate of 3γ annihilations is low, we have argued that the positronium imaging may become feasible with the advent of the total-body PET scanners. The average lifetime of positronium, as well as the fraction of its annihilations into three-photons, depend on the size of the free volumes between atoms and there are experimental indications (Jasińska et al., 2017b,a, Pietrzak et al., 2013, Liu et al., 2007) that it is correlated with the metabolic disorders of the human tissues. Therefore, imaging of the properties of positronium inside the body may deliver new in-vivo diagnostic information complementary to the standardized uptake value (SUV index).

In this article we focused our attention on the feasibility studies of imaging of the ortho-positronium mean lifetime which requires application of radiopharmaceuticals labeled with isotopes emitting a prompt gamma (e.g. ^{44}Sc). The prompt gamma is used to determine the creation time of positronium and thus the lifetime may be determined event-by-event based on the reconstructed time difference between annihilation and creation. However, the introduced method may be also used to determine images of the ratio of the rate of 3γ to 2γ annihilations

which is also sensitive to the size and concentration of free voids between atoms (Jasińska and Moskal, 2017). In this case the prompt gamma is not required and such an image may be created for all radiopharmaceuticals, independently of the kind of the used β^+ tracer.

Acknowledgments

The authors acknowledge technical and administrative support of A. Heczko, M. Kajetanowicz and W. Migdał. This work was supported by The Polish National Center for Research and Development through grant INNOTECH-K1/IN1/64/159174/NCBR/12, the Foundation for Polish Science through the MPD and TEAM/2017-4/39 programmes, the National Science Centre of Poland through grants no. 2016/21/B/ST2/01222, 2017/25/N/NZ1/00861, the Ministry for Science and Higher Education through grants no. 6673/IA/SP/2016, 7150/E-338/SPUB/2017/1 and 7150/E-338/M/2017, 7150/E-338/M/2018 and the Austrian Science Fund FWF-P26783.

References

- Abuelhia E, Kacperski K and Spyrou N 2007 Three-photon annihilation in pet: 2d imaging experiments *Journal of Radioanalytical and Nuclear Chemistry* **271**(2), 489–495.
- Al-Ramadhan A H and Gidley D W 1994 New precision measurement of the decay rate of singlet positronium *Phys. Rev. Lett.* **72**, 1632–1635.
- Axpe E, Lopez-Euba T, Castellanos-Rubio A, Merida D, Garcia J A, Plaza-Izurieta L, Fernandez-Jimenez N, Plazaola F and Bilbao J R 2014 Detection of atomic scale changes in the free volume void size of three-dimensional colorectal cancer cell culture using positron annihilation lifetime spectroscopy *PLOS ONE* **9**(1), 1–5.
- Becker R *et al.* 2017 The SAFIR experiment: Concept, status and perspectives *Nuclear Instruments and Methods in Physics Research Section A: Accelerators, Spectrometers, Detectors and Associated Equipment* **845**, 648–651.
- Cal-González J, Lage E, Herranz E, Vicente E, Udias J M, Moore S C, Park M A, Dave S R, Parot V and Herraiz J L 2015 Simulation of triple coincidences in pet *Physics in Medicine and Biology* **60**(1), 117.
- Chen H, Van Horn J and Ching Jean Y 2012 Applications of positron annihilation spectroscopy to life science **331**, 275–293.
- Cherry S R, Badawi R D, Karp J S, Moses W W, Price P and Jones T 2017 Total-body imaging: Transforming the role of positron emission tomography *Science Translational Medicine* **9**(381).
- Cherry S R, Jones T, Karp J S, Qi J, Moses W and Badawi R 2017 Total-body pet: maximizing sensitivity to create new opportunities for clinical research and patient care *Journal of Nuclear Medicine* **59**, 3–12.
- Coleman P 2000 *Positron beams and their applications* World Scientific Singapore.

- Conti M 2009 State of the art and challenges of time-of-flight pet *Physica Medica* **25**, 1–11.
- Donnard J, Chen W T, Cussonneau J P, Duval S, Lamblin J, Lemaire O, Hadi A F M, Ray P L, Morteau E, Oger T, Lavina L S, Stutzmann J S and Thers D 2012 Compton imaging with liquid xenon and 44sc: recent progress toward 3 gamma imaging *Nuclear Medicine Review* **15**(C), 64–67.
- Dulski K *et al.* 2018 Commissioning of the j-pet detector in view of the positron annihilation lifetime spectroscopy *Hyperfine Interactions* **239**, 40.
- Eldrup M, Lightbody D and Sherwood J 1981 The temperature dependence of positron lifetimes in solid pivalic acid *Chemical Physics* **63**(1), 51 – 58.
- Eriksson L and Conti M 2015 Randoms and tof gain revisited *Physics in Medicine and Biology* **60**, 1613–1623.
- Gajos A *et al.* 2016 Trilateration-based reconstruction of ortho-positronium decays into three photons with the J-PET detector *Nucl. Instrum. Meth.* **A819**, 54–59.
- Garwin R L 1953a Thermalization of positrons in metals *Phys. Rev.* **91**, 1571–1572.
- Garwin R L 1953b Thermalization of positrons in metals *Phys. Rev.* **91**, 1571–1572.
- Goworek T, Ciesielski K, Jasińska B and Wawryszczuk J 1997 Positronium in large voids. silicagel *Chemical Physics Letters* **272**(1), 91 – 95.
- Goworek T, Ciesielski K, Jasińska B and Wawryszczuk J 1998 Positronium states in the pores of silica gel *Chemical Physics* **230**(2), 305 – 315.
- Goworek T, Rybka C, Wasiewicz R and Wawryszczuk J 1982 Positronium trapping at thermally produced defects in naphthalene *physica status solidi (b)* **113**(1), K9–K13.
- Grignon C, Barbet J, Bardiès M, Carlier T, Chatal J, Couturier O, Cussonneau J, Faivre A, Ferrer L, Girault S, Haruyama T, Ray P L, Luquin L, Lupone S, Métivier V, Morteau E, Servagent N and Thers D 2007 Nuclear medical imaging using $\beta + \gamma$ coincidences from 44sc radio-nuclide with liquid xenon as detection medium *Nuclear Instruments and Methods in Physics Research Section A: Accelerators, Spectrometers, Detectors and Associated Equipment* **571**(1), 142 – 145. Proceedings of the 1st International Conference on Molecular Imaging Technology.
- Harpen M D 2004 Positronium: Review of symmetry, conserved quantities and decay for the radiological physicist *Medical Physics* **31**(1), 57–61.
- Hofman M S, Kong G, Neels O C, Eu P, Hong E and Hicks R J 2012 High management impact of ga-68 dotatate (gatate) pet/ct for imaging neuroendocrine and other somatostatin expressing tumours *Journal of Medical Imaging and Radiation Oncology* **56**(1), 40–47.
- Huclier-Markai S, Kerdjoudj R, Alliot C, Bonraisin A, Michel N, Haddad F and Barbet J 2014 Optimization of reaction conditions for the radiolabeling of dota and dota-peptide with 44m/44sc and experimental evidence of the feasibility of an in vivo pet generator *Nuclear Medicine and Biology* **41**(Supplement), e36 – e43.
- Jasinska B, Dawidowicz A L and Pikus S 2003 Application of positron annihilation lifetime spectroscopy in studies of crystallization processes *Phys. Chem. Chem. Phys.* **5**, 3289–3293.

- Jasińska B and Dawidowicz A 2003 Pore size determination in vycor glass *Radiation Physics and Chemistry* **68**(3), 531 – 534. Proceedings of the 7th International Conference on Positron and Positronium Chemistry.
- Jasińska B *et al.* 2017a Human Tissue Investigations Using PALS Technique — Free Radicals Influence *Acta Phys. Polon.* **A132**, 1556.
- Jasińska B *et al.* 2017b Human Tissues Investigation Using PALS Technique *Acta Phys. Polon.* **B48**, 1737.
- Jasińska B and Moskal P 2017 A new PET diagnostic indicator based on the ratio of $3\gamma/2\gamma$ positron annihilation *Acta Phys. Polon.* **B48**, 1577.
- Jean Y C and Ache H J 1977 Studies of molecular association in biological systems by positron annihilation techniques *Journal of the American Chemical Society* **99**(5), 1623–1625.
- Jean Y, Chen H, Liu G and Gadzia J E 2007 Life science research using positron annihilation spectroscopy: UV-irradiated mouse skin *Radiation Physics and Chemistry* **76**(2), 70 – 75. Proceedings of the 8th International Workshop on Positron and Positronium Chemistry.
- Jean Y, Li Y, Liu G, Chen H, Zhang J and Gadzia J E 2006 Applications of slow positrons to cancer research: Search for selectivity of positron annihilation to skin cancer *Applied Surface Science* **252**(9), 3166 – 3171. Proceedings of the Tenth International Workshop on Slow Positron Beam Techniques for Solids and Surfaces.
- Jinnouchi O, Asai S and Kobayashi T 2003 Precision measurement of orthopositronium decay rate using SiO(2) powder *Phys. Lett.* **B572**, 117–126.
- Kacperski K and Spyrou N M 2005 Performance of three-photon pet imaging: Monte carlo simulations *Physics in Medicine and Biology* **50**(23), 5679.
- Kacperski K, Spyrou N M and Smith F A 2004 Three-gamma annihilation imaging in positron emission tomography *IEEE Transactions on Medical Imaging* **23**(4), 525–529.
- Kamińska D *et al.* 2016 A feasibility study of ortho-positronium decays measurement with the J-PET scanner based on plastic scintillators *Eur. Phys. J.* **C76**(8), 445.
- Kobayashi Y, Zheng W, Meyer E F, McGervey J D, Jamieson A M and Simha R 1989 Free volume and physical aging of poly(vinyl acetate) studied by positron annihilation *Macromolecules* **22**(5), 2302–2306.
- Korcyl G *et al.* 2016 Sampling FEE and Trigger-less DAQ for the J-PET Scanner *Acta Phys. Polon.* **B47**, 491.
- Korcyl G *et al.* 2018 Evaluation of single chip real time tomographic data processing on fpga soc devices *IEEE Transactions on Medical Imaging* **37**(11), 2526–2535.
- Kowalski P *et al.* 2015 Multiple scattering and accidental coincidences in the j-pet detector simulated using gate package *Acta Phys. Polon* **A127**, 1505–1512.
- Kowalski P *et al.* 2016 Scatter fraction of the j-pet tomography scanner *Acta Phys. Polon* **B47**, 549.
- Kowalski P *et al.* 2018 Estimating the nema characteristics of the j-pet tomograph using the gate package *Phys. Med. Biol.* **63**, 165008.

- Krajewski S *et al* . 2013 Cyclotron production of ^{44}Sc for clinical application *Radiochimica Acta International journal for chemical aspects of nuclear science and technology* **101**(5), 333–338.
- Krzemień W *et al* . 2015 Analysis framework for the J-PET scanner *Acta Phys. Polon.* **A127**, 1491–1494.
- Kubicz E *et al* . 2015 Studies of unicellular micro-organisms *Saccharomyces cerevisiae* by means of Positron Annihilation Lifetime Spectroscopy *Nukleonika* **60**, 749–753.
- Lang C, Habs D, Parodi K and Thirolf P G 2014 Sub-millimeter nuclear medical imaging with high sensitivity in positron emission tomography using $\beta^+\gamma$ coincidences *Journal of Instrumentation* **9**(01), P01008.
- Lang C, Habs D, Thirolf P G and Zoglauer A 2012 Submillimeter nuclear medical imaging with a Compton Camera using triple coincidences of collinear β^+ annihilation photons and γ -rays.
- Lecoq P 2017 Pushing the limits in time-of-flight pet imaging *IEEE Transactions on Radiation and Plasma Medical Sciences* **1**(6), 473–485.
- Lin H H, Chuang K S, Chen S Y and Jan M L 2016 Recovering the triple coincidence of non-pure positron emitters in preclinical pet *Physics in Medicine and Biology* **61**(5), 1904.
- Liu G, Chen H, Chakka L, Cheng M L, Gadzia J E, Suzuki R, Ohdaira T, Oshima N and Jean Y 2008 Further search for selectivity of positron annihilation in the skin and cancerous systems *Applied Surface Science* **255**(1), 115–118. Proceedings of the Eleventh International Workshop on Slow Positron Beam Techniques for Solids and Surfaces.
- Liu G, Chen H, Chakka L, Gadzia J E and Jean Y C 2007 Applications of positron annihilation to dermatology and skin cancer *physica status solidi (c)* **4**(10), 3912–3915.
- Moskal P *et al* . 2013 ‘TOF-PET tomograph and a method of imaging using a TOF-PET tomograph, based on a probability of production and lifetime of a positronium’. Patent US 9851456 (2017), PL 227658 (2013).
- Moskal P *et al* . 2014 Test of a single module of the J-PET scanner based on plastic scintillators *Nucl. Instrum. Meth.* **A764**, 317–321.
- Moskal P *et al* . 2015 A novel method for the line-of-response and time-of-flight reconstruction in TOF-PET detectors based on a library of synchronized model signals *Nucl. Instrum. Meth.* **A775**, 54–62.
- Moskal P *et al* . 2016 Time resolution of the plastic scintillator strips with matrix photomultiplier readout for J-PET tomograph *Phys. Med. Biol.* **61**, 2025.
- National Nuclear Data Center 2016 <http://www.nndc.bnl.gov/>. Accessed: 20.01.2016.
- NEMA 2012 ‘Performance measurements of positron emission tomographs’. National Electrical Manufacturers Association (NEMA NU 2-2012).
- Nemallapudi M V, Gundacker S, Lecoq P, Auffray E, Ferri A, Gola and Piemonte C 2015 Sub-100 ps coincidence time resolution for positron emission tomography with Iso:ce codoped with ca *Physics in Medicine and Biology* **60**(12), 4635.

- Niedźwiecki S *et al* . 2017 J-PET: a new technology for the whole-body PET imaging *Acta Phys. Polon.* **B48**, 1567.
- NUCLEIDE-LARA - Library for alpha, X and gamma emissions 2017 <http://www.nucleide.org/NucData.htm>. Accessed: 10.02.2018.
- Oger T *et al* . 2012 A Liquid xenon TPC for a medical imaging Compton telescope *Nucl. Instrum. Meth.* **A695**, 125–128.
- Pawlik-Niedźwiecka M *et al* . 2017 Preliminary Studies of J-PET Detector Spatial Resolution *Acta Phys. Polon.* **A132**, 1645.
- Pałka M *et al* . 2017 Multichannel FPGA based MVT system for high precision time (20 ps RMS) and charge measurement *JINST* **12**(08), P08001.
- Pietrzak R, Borbulak S and Szatanik R 2013 Influence of neoplastic therapy on the investigated blood using positron annihilation lifetime spectroscopy *Nukleonika* **Vol. 58, No. 1**, 199–202.
- Pizzichemi M *et al* . 2016 A new method for depth of interaction determination in PET detectors *Physics in Medicine and Biology* **61**(12), 4679.
- Schaart D R *et al* . 2010 Labr 3 :ce and sipms for time-of-flight pet: achieving 100 ps coincidence resolving time *Physics in Medicine and Biology* **55**(7), N179.
- Schrader D M and Jean Y C 1988 *Positron and Positronium Chemistry* Elsevier.
- Shopa R Y *et al* . 2017 Three-dimensional image reconstruction in j-pet using filtered back-projection method *Acta Phys. Polon. B* **48**, 1757.
- Singh A *et al* . 2017 First-in-human pet/ct imaging of metastatic neuroendocrine neoplasms with cyclotron-produced 44sc-dotatoc: A proof-of-concept study *Cancer Biotherapy & Radiopharmaceuticals* **32**(4), 124–132.
- Slomka P J, Pan T and Germano G 2016 Recent advances and future progress in pet instrumentation *Seminars in Nuclear Medicine* **46**(1), 5 – 19. Recent Advances and Future Perspectives in Nuclear Medicine.
- Stepanov S *et al* . 2011 Incorporation of the magnetic quenching effect into the blob model of ps formation. finite sized ps in a potential well in ‘Progress in Positron Annihilation’ Vol. 666 of *Materials Science Forum* Trans Tech Publications pp. 109–114.
- Stepanov S, Zvezhinskiy D, Duplâtre G, Byakov V, Yu. Batskikh Y and Stepanov P 2010 Incorporation of the magnetic quenching effect into the blob model of ps formation. finite sized ps in a potential well **666**, 109–114.
- Szkliniarz K *et al* . 2015 Medical radioisotopes produced using the alpha particle beam from the warsaw heavy ion cyclotron *Acta Phys. Polon.* **A127**, 1471.
- Tao S J 1972 Positronium annihilation in molecular substances *The Journal of Chemical Physics* **56**(11), 5499–5510.
- Thielemans K, Tsoumpas C, Mustafovic S, Beisel T, Aguiar P, Dikaios N and Jacobson M W 2012 STIR: software for tomographic image reconstruction release 2 *Physics in Medicine and Biology* **57**(4), 867.

- Thirolf P G, Lang C and Parodi K 2015 Perspectives for highly-sensitive pet-based medical imaging using $\beta^+\gamma$ coincidences *Acta Phys. Pol. A*(127), 1441–1444.
- Townsend D W 2008 Multimodality imaging of structure and function *Physics in Medicine and Biology* **53**, R1–R39.
- Vallery R S, Zitzewitz P W and Gidley D W 2003 Resolution of the orthopositronium-lifetime puzzle *Phys. Rev. Lett.* **90**, 203402.
- van Dam H T *et al* . 2011 A practical method for depth of interaction determination in monolithic scintillator PET detectors *Physics in Medicine and Biology* **56**(13), 4135.
- Vandenberghe S, Mikhaylova E, D’Hoe E, Mollet P and Karp J S 2016 Recent developments in time-of-flight pet *EJNMMI Physics* **3**(1), 3.
- Viswanath V *et al* . 2017 Development of PET for Total-Body Imaging *Acta Phys. Polon.* **B48**, 1555.
- Walczak R, Krajewski S, Szkliniarz K, Sitarz M, Abbas K, Choiński J, Jakubowski A, Jastrzebski J, Majkowska A, Simonelli F, Stolarz A, Trzcińska A, Zipper W and Bilewicz A 2015 Cyclotron production of ^{43}Sc for pet imaging *EJNMMI Physics* **2**(1), 33.
- Yan J, Schaefferkoetter J, Conti M and Townsend D 2016 A method to assess image quality for low-dose pet: analysis of snr, cnr, bias and image noise *Cancer Imaging* **16**(1), 26.
- Yas R M, Al-Mshhdani A H, M.Elias M and Al-Sheibani Z T 2012 Detection of line shape parameters in normal and abnormal biological tissues *Iraqi Journal of Physics* **10**(17), 77–82.
- Zhang X, Zhou J, Cherry S R, Badawi R D and Qi J 2017 Quantitative image reconstruction for total-body pet imaging using the 2-meter long explorer scanner *Physics in Medicine & Biology* **62**(6), 2465.